

FIBRE-OPTIC SENSORS

https://doi.org/10.1070/QEL17225

Measurement accuracy and spatial resolution of a distributed temperature sensor based on a two-pulse differential coherent reflectometer

T.O. Lukashova, O.E. Nanii, S.P. Nikitin, V.N. Treshchikov

Abstract. **We present a model and numerical simulation of a distributed temperature sensor based on a two-pulse differential coherent optical time-domain reflectometer (COTDR). The differential phase measured using a phase-sensitive Rayleigh reflectometer is shown to have a regular component, which is a linear function of temperature, and a random component, which is related to a random distribution of scattering centres in the fibre and restricts the accuracy of measurements of variations in temperature. Measurement accuracy can be improved by reducing the relative contribution of the random component via a decrease in pulse duration and/or an increase in the time delay between pulses. The spatial resolution of a differential two-pulse phase-sensitive reflectometer is shown to be determined by the time delay between pulses and to vary little with pulse duration. At a typical pulse duration (200 ns) and delay time (300 ns), the accuracy in measurements of variations in temperature in the 0.1-K range is 2% and the spatial resolution is about 30 m.**

Keywords: *optical time-domain reflectometer, Rayleigh temperature sensor, phase-sensitive reflectometer, spatial resolution, measurement accuracy.*

1. Introduction

In the past few decades, distributed fibre-optic sensors (DFOS's) have been widely used to resolve issues pertaining to the monitoring of infrastructure facilities and parameters of natural or artificial external physical fields acting on them.

The most in-demand DFOS's are those for temperature, stress, and vibration measurements: distributed temperature sensors (DTS's), distributed stress sensors (DSS's), and distributed acoustic or vibration sensors (DAS's/DVS's) [1, 2], in which standard telecom optical fibre is used as a sensing element. Traditionally, spontaneous Raman scattering (SRS) is used in the DTS's [3–5]; spontaneous (or stimulated) Brillouin scattering (SBS) [6, 7], also temperature-sensitive, is used in the DSS's; and Rayleigh scattering is used in the DAS's/DVS's [8–11].

It is very tempting to use Rayleigh scattering-based DFOS's for distributed temperature measurements. The feasibility of this approach, based on the detection of temperature-induced changes in the interference structure of scattered light, was demonstrated by Rathod et al. [12] and Froggatt and Moore [13], who used reflectometers with frequency modulation of probe light: optical frequency domain reflectometry (OFDR). However, the short operation range of OFDR limits potential application areas of such devices.

Koyamada et al. [14, 15] proposed and experimentally demonstrated a correlation method of distributed temperature measurements with the use of coherent optical time-domain reflectometers (COTDRs). The principle of temperature measurements with a COTDR is based on the existence of a correlation between reflectograms obtained at a probe pulse frequency shift and a temperature change: reflectograms in which frequency and temperature shifts are related in a certain way are as similar in shape as possible. However, practical implementation of a correlation OTDR for temperature measurements is hindered by the long measurement time, the complexity of signal processing algorithms, and stringent requirements for performance characteristics of the components involved.

It is only very recently that Nikitin et al. [16] have experimentally implemented a DTS based on a differential two-pulse COTDR that meets requirements for industrial application in terms of both sensitivity and operation range.

This paper presents the first model and numerical simulation of a DTS based on a two-pulse differential COTDR operating according to a scheme proposed by Treshchikov et al. [17]. Previously reported theoretical and experimental studies examined only DAS's/DVS's based on single-pulse COTDRs [18–24]. It was not analysed in those reports whether the types of COTDRs examined were applicable to temperature measurements.

2. Model of scattering

A numerical model of scattered light relies on the following propositions:

1. The time sample spacing, $dt = 1$ ns, is chosen to be much smaller than the probe pulse duration, $t_p = 200$ ns:

$$dt \ll t_p. \tag{1}$$

T.O. Lukashova T8 Scientific and Technical Center LLC, Krasnobogatyrskaya ul. 44/1, 107076 Moscow, Russia; e-mail: lukashova@t8.ru;
O.E. Nanii T8 Scientific and Technical Center LLC, Krasnobogatyrskaya ul. 44/1, 107076 Moscow, Russia; Faculty of Physics, M.V. Lomonosov Moscow State University, Vorob'evy gory, 119324 Moscow, Russia;
S.P. Nikitin T8 Sensor LLC, Krasnobogatyrskaya ul. 44/1, 107076 Moscow, Russia;
V.N. Treshchikov T8 Scientific and Technical Center LLC, Krasnobogatyrskaya ul. 44/1, 107076 Moscow, Russia; Kotelnikov Institute of Radioengineering and Electronics (Fryazino Branch), Russian Academy of Sciences, pl. Vvedenskogo 1, 141190 Fryazino, Moscow region, Russia

Received 12 December 2019; revision received 14 February 2020
Kvantovaya Elektronika **50** (9) 882–887 (2020)
Translated by O.M. Tsarev

2. In a real fibre, the number of scattering centres (SCs) is large, but Rayleigh scattering parameters can be described with sufficient accuracy by a small number of such centres. To speed up computations, the model contains the minimum number of scatterers at which the main statistical characteristics of scattered light still persist. This condition is well fulfilled if the number of SCs per sample spacing is ten. A time sample spacing of 1 ns corresponds to a spatial spacing of 10 cm, so the average density of SC arrangement was taken to be 1 cm^{-1}.

3. A change in fibre temperature leads to a change in relative phase shifts of partial waves scattered by different SCs. Such changes in relative phase shifts are due to both temperature variations of the refractive index of the fibre and the shift of the position of the SCs as a result of its thermal expansion. In our model, a real variation in the refractive index and expansion are replaced by the variation in an equivalent refractive index:

$$n_{eq}(T) = n_0 + n_0\beta(T - T_0), \tag{2}$$

$$\beta = \mu + \chi = 9.15 \times 10^{-6}\ \mathrm{K}^{-1}, \tag{3}$$

where n_0 is the refractive index (RI) at the initial temperature T_0; μ is the thermo-optic coefficient (that of quartz is $\sim 8.6 \times 10^{-6}\ \mathrm{K}^{-1}$); and χ is the thermal expansion coefficient ($\sim 0.55 \times 10^{-6}\ \mathrm{K}^{-1}$) [25].

3. Model of a coherent reflectometer

Figure 1 shows a schematic of a COTDR. The probe pulse shape is described by the function $E_0(t)$. Probe light backscattering by each SC in the sensing fibre produces partial scattered waves, and their constructive or destructive interference yields a reflectogram. The complex amplitude of the reflectogram at time t is the sum of partial signals backscattered by scattering centres with coordinates ξ_m at instants in time before t by

$$\frac{2\int_0^{\xi_m} n(z)\,dz}{c}$$

(the time needed for light to propagate to the SC and back):

$$E(t) = \sum_{m=1}^{M} \sqrt{a}\,E_0\left(t - \frac{2\int_0^{\xi_m} n(z)\,\mathrm{d}z}{c}\right)\exp\left(2ik\int_0^{\xi_m} n(z)\,\mathrm{d}z\right), \tag{4}$$

where the coefficient a determines the fraction of the power of the backscattered light propagating in the mode ($a = 2 \times 10^{-4}$ for single-mode fibre); $n(z)$ is the spatial RI profile along the fibre; $c = 3 \times 10^9\ \mathrm{m\ s^{-1}}$ is the speed of light in vacuum; $k = 2\pi/\lambda$ is the wavenumber corresponding to the wavelength $\lambda = 1.55\ \mu\mathrm{m}$; and M is the total number of SCs in the fibre section under study.

An external influence changes the position of scattering centres and/or the refractive index $n(z)$, leading to a change in the complex amplitude $E(t)$. A reflectogram shows the photodetector current as a function of time: $X(t) \sim |E(t)|^2$.

Using this model and the MATLAB environment, we wrote a program simulating the operation of a COTDR. The program allows one to perform calculations for various pulse shapes, with allowance for signal attenuation. The influence of nonlinear effects is left out of consideration.

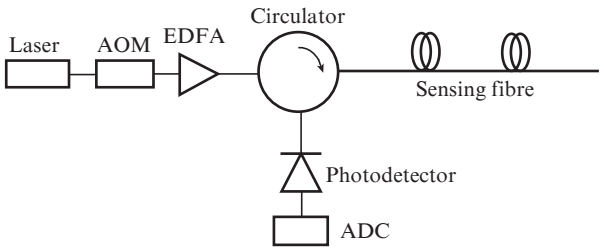

Figure 1. Schematic of a COTDR. The laser and acousto-optic modulator (AOM) produce a probe coherent light pulse or a pair of pulses, the erbium-doped fibre amplifier (EDFA) amplifies the signal before it enters the sensing fibre, and the circulator directs the backscattered signal to a photodetector connected to an ADC.

The operating principle of a differential phase-sensitive coherent reflectometer is to measure the phase difference $\Delta\varphi$ between reflectograms of two pulses, which in what follows will be referred to as a differential phase:

$$\Delta\varphi = \varphi_1 - \varphi_2. \tag{5}$$

It should be emphasised that, in the two-pulse configuration, one determines the phase difference ($\Delta\varphi$) rather than the absolute phase.

The model of scattering for rectangular probe pulses is illustrated by Fig. 2.

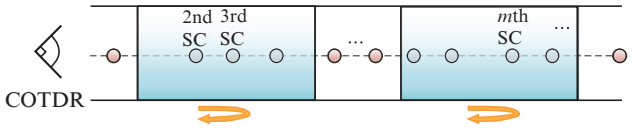

Figure 2. Model of scattering for rectangular probe pulses.

The temperature distribution in the fibre, $T(z)$, varies stepwise, with a constant step $\mathrm{d}T$. The total variation in temperature, $\Delta T_j(z)$, is proportional to the number of steps, j:

$$\Delta T_j(z) = T_j - T_0 = \mathrm{d}Tj,\ j = 0, \ldots, m. \tag{6}$$

The temperature step $\mathrm{d}T$ is chosen such that the change in the phase shift of scattered light does not exceed $\pi/10$.

The principle of measuring the differential phase was described elsewhere [16, 17]. It consists in probing fibre by a sequence of four pairs of pulses. The second pulse has a fixed delay τ, and the phase shift between the pulses in a pair is periodically changed so that it takes values of 0, $\pi/2$, π, and $3\pi/2$ (Fig. 3). One measures four reflectograms, i.e. time dependences of the photodetector current: $X_i(t)$, where $i = 1-4$. Using the four reflectograms [$X_1(t)$, $X_2(t)$, $X_3(t)$, and $X_4(t)$] obtained from the pairs of probe pulses, one calculates the differential phase $\Delta\varphi(t)$, which is a function of time t, moreover, a random function, and is represented as a phase reflectogram: differential phase as a function of signal delay time. The relations between $\Delta\varphi(t)$ and reflectograms have the following form:

$$\sin(\Delta\varphi) = \frac{X_4 - X_2}{4\sqrt{P_1 P_2}},$$
$$\cos(\Delta\varphi) = \frac{X_1 - X_3}{4\sqrt{P_1 P_2}} \Rightarrow \tan(\Delta\varphi) = \frac{X_4 - X_2}{X_1 - X_3}. \quad (7)$$

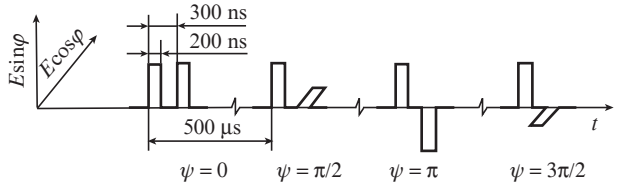

Figure 3. Two-pulse COTDR scheme.

Since the system initially has some nonzero differential phase at the initial temperature T_0, it is convenient to describe variations in temperature using the quantity

$$\Delta\tilde{\varphi}_i(t, T_i) = \Delta\varphi(t, T_i) - \Delta\varphi(t, T_0). \quad (8)$$

It will be referred to as the temperature variation of the differential phase.

The nominal temperature variation of the differential phase between signals scattered by two scattering regions (Fig. 2) is described by the following relation [16]:

$$\Delta\tilde{\varphi} = \frac{2\pi c\tau}{\lambda}\beta\Delta T \equiv \alpha\Delta T. \quad (9)$$

The proportionality coefficient between the differential phase and the variation in temperature is

$$\alpha = \frac{2\pi c\tau}{\lambda}\beta. \quad (10)$$

For example, at standard parameters of an acousto-optic reflectometer ($\tau = 300$ ns, $\lambda = 1.55$ μm, and $\beta = 9.15 \times 10^{-6}$ K^{-1}) we obtain in the case of two scattering regions $\alpha_{est} = 3348$ rad K^{-1}.

4. Numerical simulation parameters

In this study, we numerically simulate the two-pulse configuration that was studied experimentally by Nikitin et al. [16]. Numerical simulation was carried out with parameters indicated below.

Pulse duration, t_p/ns	200
Delay time, τ/ns	300
Time sample spacing, dt/ns	1
Wavelength, λ/nm	1550
Number of SCs/m^{-1}	100
Initial RI, n_0	1.45
Temperature step, dT/mK	0.1

The temperature step, d$T = 0.1$ mK, was chosen such that the change in the differential phase did not exceed $\pi/10$. To exclude uncertainty in calculating the phase $\Delta\varphi$ from a tangent, $\Delta\varphi = \arctan x \pm m\pi$ (where m is an integer), we applied the phase continuity constraint, which is implemented in practice by the unwrapping algorithm [26].

5. Simulation results

5.1. Differential phase as a function of variation in temperature

The slope of the dependence of the temperature variation of the differential phase, $\Delta\tilde{\varphi}$, on the variation in temperature for five independent fibre sections (channels) is shown in Fig. 4. The calculation results approach the nominal linear dependence with a slope $\alpha_{est} = 3348$ rad K^{-1}. The differential phase has a regular component, which tends to the nominal dependence on the variation in temperature, and an irregular component, due to the random character of the distribution of SCs over the fibre.

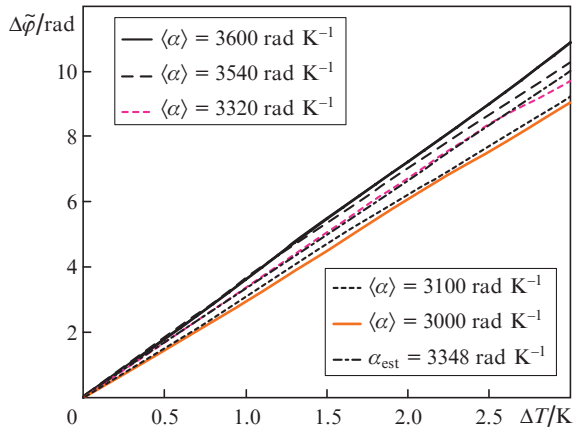

Figure 4. Temperature variation of the differential phase as a function of the variation in temperature for five independent fibre sections (channels). We present the average proportionality coefficient α for five channels. The nominal value is $\alpha_{est} = 3348$ rad K^{-1}.

5.2. Error in measurements of the variation in temperature

The relative error in measurements of the variation in temperature is defined as follows:

$$\delta(\Delta T_{meas}) = \frac{\sigma(\Delta T_{meas} - \Delta T_{nom})}{\Delta T_{nom}}, \quad (11)$$

where ΔT_{meas} is the variation in temperature measured in a numerical experiment; ΔT_{nom} is the nominal variation in temperature; and $\sigma(\Delta T_{meas} - \Delta T_{nom})$ is the standard deviation.

The numerical simulation results on the dependence of the relative error on the variation in temperature are presented in Fig. 5. It is seen that increasing the variation in temperature leads to a decrease in relative measurement error.

Figure 6 shows the relative error in measurements of the variation in temperature as a function of pulse duration at constant $\tau = 300$ ns and a variation in temperature $\Delta T = 0.4$ mK. Reducing the pulse duration also leads to decrease in measurement error.

Figure 7 shows the relative error in measurements of the variation in temperature as a function of the time delay of the second pulse relative to the first pulse at a constant pulse

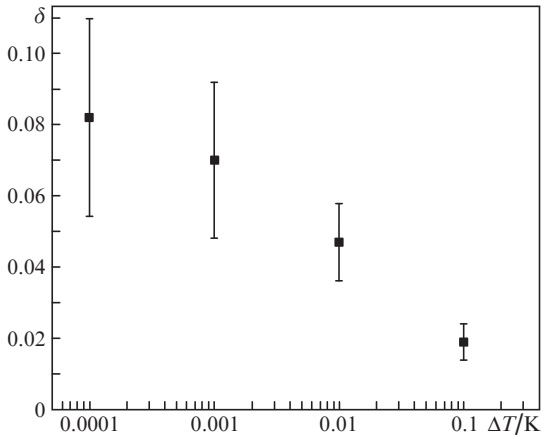

Figure 5. Relative error in measurements of variations in temperature as a function of the variation in temperature at a pulse duration t_p = 200 ns and delay time τ = 300 ns.

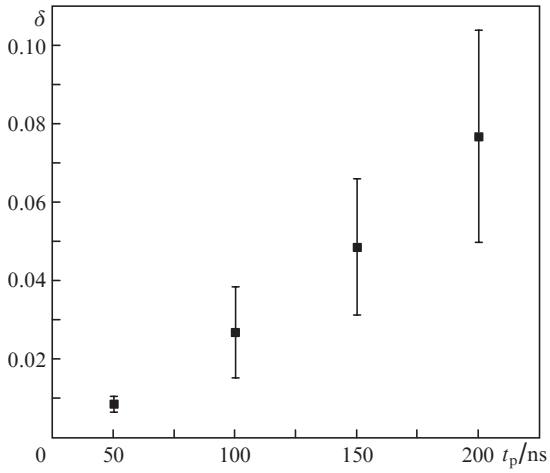

Figure 6. Relative error in measurements of variations in temperature (ΔT = 0.4 mK) as a function of probe pulse duration at constant τ = 300 ns.

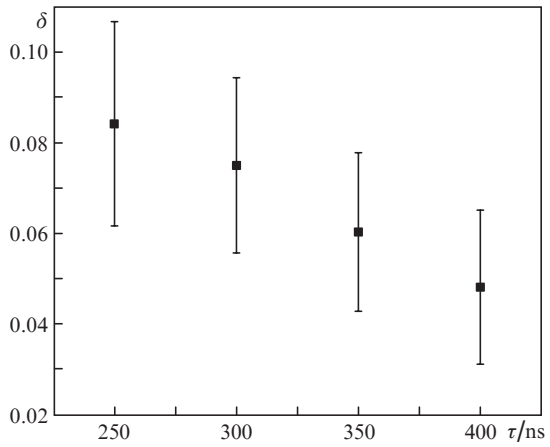

Figure 7. Relative error in measurements of variations in temperature as a function of delay time τ at a constant probe pulse duration t_p = 200 ns.

duration t_p = 200 ns (temperature range ΔT = 0.4 mK). It is seen that increasing the time delay τ reduces the error in measurements of the variation in temperature.

5.3. Spatial resolution

To assess the spatial resolution of a DTS, the temperature is set in the form of a step of height ΔT = 0.2 mK. The temperature profile calculated using our model is shown in Fig. 8. We determine spatial resolution L_{sp} as the distance between the points at which the changes in temperature are 10% and 90% of the nominal increase in temperature. Spatial resolution and its standard deviation were determined by averaging over at least 50 implementations.

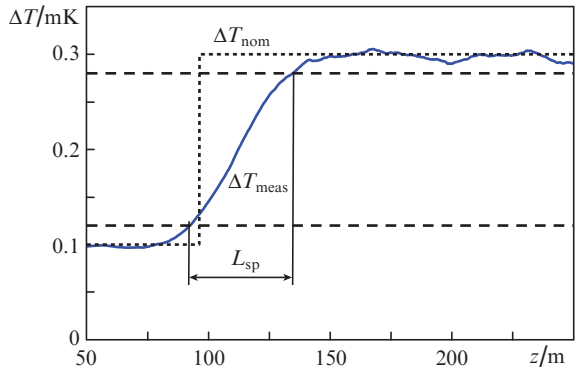

Figure 8. Illustration of the principle of estimating the spatial resolution L_{sp} of a DTS. The short-dashed line shows the given spatial profile (step) of the variation in temperature, the solid line shows the DTS signal obtained by numerical simulation, and the horizontal long-dashed lines represent the 10% and 90% levels relative to the nominal increase in temperature.

Figure 9 shows spatial resolution as a function of pulse duration at constant τ = 300 ns, and Fig. 10 shows the spatial resolution of a DTS as a function of the time delay between two pulses at a constant pulse duration t_p = 200 ns.

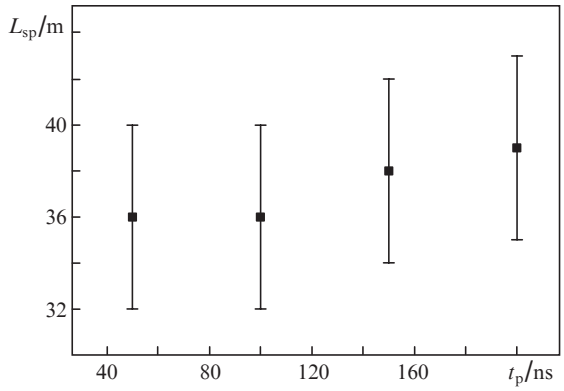

Figure 9. Spatial resolution of a DTS as a function of probe pulse duration at constant τ = 300 ns.

6. Discussion

6.1. Temperature measurement error

The principle of measuring the variation in temperature with a distributed sensor is to measure the differential phase $\Delta\varphi$

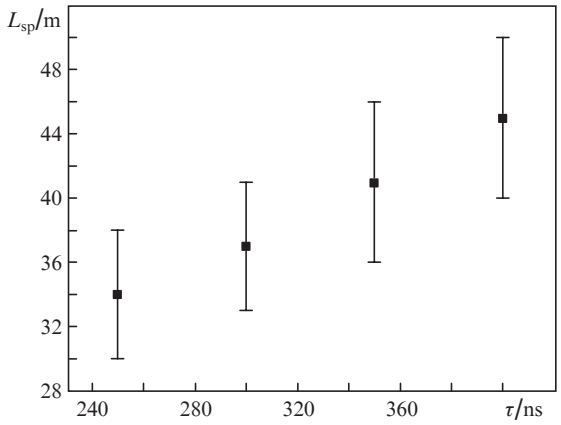

Figure 10. Spatial resolution of a DTS as a function of the time delay between two pulses at $t_p = 200$ ns.

due to the variation in temperature between the reflectograms of two fibre sections separated by

$$\Delta l = c\tau/(2n), \tag{12}$$

where n is the refractive index. The temperature variation of the differential phase has a regular component, $\Delta\varphi_{reg}$, determined by the variation in optical path length between two reflecting regions:

$$\Delta\varphi_{reg} = \alpha_{reg}\Delta T. \tag{13}$$

At the same time, the measured differential phase $\Delta\varphi = \varphi_1 - \varphi_2$ has a random (irregular) component as well, due to variations in parameters of 'irregular grids'. The irregular component originates from the random distribution of scattering centres over the fibre and restricts the accuracy of measurements of the variation in temperature.

As follows from our numerical simulations, the relative error in measurements of variations in temperature, $\delta(\Delta T_{meas})$, decreases with increasing temperature range ΔT and is 2% at $\Delta T = 0.1$ K, $t_p = 200$ ns, and $\tau = 300$ ns (Fig. 5). The decrease in measurement error with increasing ΔT can be accounted for by the fact that the regular component $\Delta\varphi_{reg}$ increases linearly with an increase in the variation in temperature, whereas the irregular component rises more slowly, usually as $\sqrt{\Delta T}$. The contribution of the irregular component to the differential phase depends on pulse duration and can be reduced, as follows from Fig. 6. At the narrow interval $\Delta T = 0.4$ K and $\tau = 300$ ns, relative error is 7.7% at $t_p = 200$ ns and 1.0% at $t_p = 50$ ns.

Another way of improving measurement accuracy is by increasing the time delay τ between the pulses in a pair (Fig. 7), but this impairs spatial resolution, as discussed below.

6.2. Spatial resolving power

Accuracy in determining the place of an external influence is characterised by the spatial resolution of the DTS. An analytical estimate of this quantity is given by the formula

$$L_{sp} = vt'/2, \tag{14}$$

where $v = c/n$ and t' is a probe signal parameter. In the case of amplitude detection, it is the pulse duration t_p; in the case of the two-pulse configuration, it is the delay time τ. For a DTS based on a phase-sensitive reflectometer and having standard parameters $t_p = 200$ ns and $\tau = 300$ ns, formula (14) gives an estimate $L_{sp} = 32$ m.

Numerical simulation results confirm the above simple estimate: the spatial resolving power of the DTS varies little with pulse duration and is proportional to the delay time (Figs 9, 10).

7. Conclusions

Using mathematical modelling, we have studied a new type of distributed temperature sensor based on a two-pulse coherent reflectometer (COTDR). We have constructed a numerical model for a distributed Rayleigh scattering-based differential temperature sensor and analysed its operation using numerical simulation.

By means of a numerical experiment, we have demonstrated high sensitivity of the distributed temperature measurement method in question, which allows one to detect temperature changes as small as a few thousandths of a degree Celsius.

At a typical pulse duration (200 ns) and delay time (300 ns), the error in measurements of variations in temperature in the 0.1-K range is 2%.

The accuracy of two-pulse measurements of an external influence on fibre has been shown to be limited by the fact that, along with the determinate component of the differential phase, there is a random component, which is determined by unpredictable variations in the scattering phases of the first and second light pulses upon changes in temperature.

The accuracy in measurements of variations in temperature can be improved by increasing the relative fraction of the regular component of the differential phase via an increase in the time delay between pulses or a decrease in the contribution of the irregular component on account of a reduction in pulse duration.

The increase in relative temperature measurement error with increasing temperature measurement range ΔT is due to the weaker dependence of the random phase shift on ΔT (1/2 power) in comparison with the linear dependence of the regular component of the phase shift on ΔT.

The spatial resolving power of the differential phase-sensitive reflectometer is determined by the time delay between pulses, varies little with pulse duration, and is ~30 m at $t_p = 200$ ns and $\tau = 300$ ns.

The method considered in this paper allows one to measure only variations in temperature rather than its absolute value. Because of this, real measurements should be made continuously over a time during which the temperature change of interest can occur.

References

1. Wang C. et al. *Opt. Commun.*, **346**, 172 (2015).
2. Tu G. et al. *IEEE Photonics Technol. Lett.*, **27** (12), 1349 (2015).
3. Dakin J., Wade C., Henning M. *Electron. Lett.*, **20** (1), 53 (1984).
4. Dakin J. et al. *Electron. Lett.*, **21** (3), 569 (1985).
5. Bolognini G., Hartog A. *Opt. Fiber Technol.*, **19** (6), 678 (2013).
6. Soto M.A., Bolognini G., Pasquale F.D. *IEEE Photonics Technol. Lett.*, **21** (7), 450 (2009).
7. Zhang H. et al. *Appl. Sci.*, **8** (10), 1820 (2018).

8. Shatalin S.V., Treschikov V.N., Rogers A.G. *Appl. Opt*., **37**, 5600 (1998).
9. He X. et al., in *Proc. 25th Opt. Fiber Sensors Conf*. (Jeju: IEEE, 2017) p. 1.
10. Hartog A., Kotov O., Liokumovich L., in *Proc. Second EAGE Workshop Permanent Reservoir 2013 – Current and Future Trends* (Stavanger: EAGE, 2013) p. 351.
11. Alekseev A.E. et al. *Quantum Electron*., **44** (10), 965 (2014) [*Kvantovaya Elektron*., **44** (10), 965 (2014)].
12. Rathod R. et al. *Opt. Lett*., **19** (8), 593 (1994).
13. Froggatt M., Moore J. *Appl. Opt*., **37** (10), 1735 (1998).
14. Koyamada Y. et al. *IEICE Trans. Commun*., **89** (5), 1722 (2006).
15. Koyamada Y. et al. *J. Lightwave Technol*., **27** (9), 1142 (2009).
16. Nikitin S. et al. *Laser Phys*., **28** (8), 085107 (2018).
17. Treshchikov V.N. et al. RF Patent No. 2562689 (2014).
18. Tosoni O. et al. *Quantum Electron*., **40** (10), 887 (2010) [*Kvantovaya Elektron*., **40** (10), 887 (2010)].
19. Liokumovich L.B. et al. *J. Lightwave Technol*., **33** (17), 3660 (2015).
20. Hartog A., Kader K. Patent US9170149B2.
21. Masoudi A., Newson T.P. *Opt. Express*, **25** (25), 32021 (2017).
22. Masoudi A., Belal M., Newson T.P. *Opt. Lett*., **38** (17), 3312 (2013).
23. Masoudi A., Belal M., Newson T.P., in *Proc. 23rd Intern. Conf. Opt. Fibre Sensors* (Santander: SPIE 9157) p. 2014.
24. Zhirnov A.A. et al. *Opt. Spectrosc*., **127** (4), 656 (2019) [*Opt. Spektrosk*., **127** (4), 603 (2019)].
25. Othonos A., Kalli K. *Fiber Bragg Gratings: Fundamentals and Applications in Telecomunications and Sensing* (London: Artech House, 1999).
26. Ghiglia D.C., Pritt M.D. *Two-dimensional Phase Unwrapping: Theory, Algorithms, and Software* (New York: Wiley-Interscience, 1998).